Density functional study on the pressure profile of the inhomogeneous fluid mixture*

Yanshuang Kang(康艳霜)[1,†], Yanmei Kang(康艳梅)[2], Zongli Sun(孙宗利)[3,‡], Yushan Li(李玉山)[4], and Shanshan Tan(檀姗姗)[3]

[1] *College of Science, Agriculture University of Hebei, Baoding* 071001, *China*
[2] *University of International Relations, Beijing* 100091, *China*
[3] *Science and Technology College, North China Electric Power University, Baoding* 071051, *China*
[4] *Department of Physics and Electronic Engineering, Heze University, Heze* 274015, *China*

(Received 10 March 2017; revised manuscript received 2 May 2017; published online 20 June 2017)

By using the statistical mechanics, the pressure tensor for the multi component fluid mixture is derived. With the help of the classical density functional theory, profiles of the pressure components are calculated, and the influence of the total volume fraction, ratio of volume fraction, and size asymmetry on the pressure are studied. In addition, our results show that for the mixture confined in the hard cavity, the pressure shows a discontinuity near the cavity wall. However, in the soft cavity condition, the discontinuity disappears.

Keywords: pressure tensor, density functional theory, fluid mixture, correlation

PACS: 61.20.Gy, 62.10.+s **DOI:** 10.1088/1674-1056/26/8/086101

1. Introduction

In statistical mechanics for systems in, or out of equilibrium, the pressure tensor is one of the most basic thermodynamic quantities because it relates not only to the mechanical equilibrium,[1] but also to the mechanical behavior in the transport process and hydrodynamics of the fluids.[2,3] Theoretically, the pioneering work on the inhomogeneous pressure tensor was conducted by Irving and Kirkwood (IK),[4] who interpreted it from a microscopic point of view. Since then, the local pressure tensor for fluids confined in different geometries had been reported in a large number of literatures, most of which were based on the IK definition.[5–8] However, latter by Schofield and Henderson,[9] it was pointed out that no unique definition for the pressure tensor exists due to the arbitrary paths connecting each pair of particles belonging to the system. The most representative alternative is the one proposed by Harasima.[10] Recently, some other novel alternative expressions for pressure tensor have also been proposed,[11–18] including the method of plane[19] and volume averaging.[20]

In a previous work,[21] two of the present authors have expressed the local pressure tensor as a functional of the density functions, which can be readily obtained from the calculation based on the density functional theory (DFT). In the study for the pure fluids, very good agreement has been observed in the comparison of the theoretical results with that from the simulation. In this work, we focus on a multi-component fluid mixture, which contains more complex correlations. It is believed that the present work on the multi-component systems may show richer information about the pressure tensor, which may be useful for us to understand the dynamic processes or behaviors in the fluid mixture.

Actually, some works exist about the pressure or stress tensor of multi-component fluids. By considering the equations of each component, Bearman and Kirkwood derived the partial molecular stress tensor of multi-component mixture based on statistical mechanics.[22] Through the perturbation solution of the modified Boltzmann equation, Harris and Rice studied the fluxes of mass, momentum, and energy in a mixture.[23] Particularly, their derivation is performed in the general case, in which the asymmetries in both mass and radius had been taken into account. Snell *et al.* provided a new microscopic theory of hydrodynamic flow, which gave a macroscopic phenomenological interpretation.[24] Compared to the results of Bearman and Kirkwood, their derivation employed a different treatment about the perturbed portion of the pair correlation function. Though so many theoretical works had been reported, to the best of our knowledge, few numerical results for the pressure tensor in multi-component fluids are available. To this end, this work aims to perform numerical calculations for the pressure in confined fluid mixtures, and then investigate the properties of the pressure tensor in them.

For convenience in the calculations, it is better to express

*Project supported by the National Natural Science Foundation of China (Grant No. 21503077), the Fundamental Research Fund for the Central Universities of China (Grant Nos. 2016MS156 and 13MS105), the Technology Research and Development Program of Hebei Province, China (Grant No. 13213704), and the Program of Study Abroad for Young Teachers by Agricultural University of Hebei.

†Corresponding author. E-mail: kang_yanshuang@163.com
‡Corresponding author. E-mail: sunzl@ncepu.edu.cn

© 2017 Chinese Physical Society and IOP Publishing Ltd

the pressure tensor as a functional of the density function. Thus, the densities of the mixture should be firstly obtained before the further calculation for pressure. Actually, one of the most powerful and popular tools for inhomogeneous fluids or their mixtures is the DFT.[25–27] However, due to the lack of knowledge about the exact expression for the excess Helmholtz free energy for most of the practical systems, some density functional approximation (DFA) is needed to implement the calculation. In fact, many DFAs including functional perturbation expansion approximation (FPEA),[28–30] bridge density functional approximation (BDFA),[31–34] weight density approximation (WDA),[35,36] and fundamental measure theory (FMT)[37] have been developed. Among them, FMT and its modified version (MFMT)[38,39] have become the fundamental starting point in the studies of the inhomogeneous fluids and mixtures.[40–43]

The paper is organized as follows. In Section 2, the pressure tensor for the fluid mixture is theoretically derived based on the statistical mechanics. In Section 3, employing the density functional theory for the fluid mixture, the normal and tangential components of the pressure tensor of the binary hard sphere fluids confined in a hard cavity are calculated and analyzed. The influences of total volume fraction, the ratio of volume fraction and size asymmetry on the pressure profile are discussed in detail. In addition, the system in a soft cavity is also calculated and analyzed in this section. A short summary is given in the last section.

2. Theory and methods

The system under consideration is a t-component fluid mixture. The ν-th component is composed by N_ν identical particles of the diameter σ_ν, with $\nu = 1,\ldots,t$ the index to distinguish the component. The mixture is confined in a volume $\boldsymbol{V}$ and the total number of particles is $N = \sum_\nu N_\nu$. The pair potential between particles i and j is denoted by $\varphi(r_i, r_j)$. For convenience, choose arbitrarily from the system a closed part with volume $\boldsymbol{G}$ and boundary $\boldsymbol{S}$. According to the hydrodynamic equation, the force acting on $\boldsymbol{S}$ due to the rate of change of the momentum, say $\boldsymbol{F}$, relates to the stress tensor $\mathbb{T}$ via the expression:

$$\boldsymbol{F} = \int_{\boldsymbol{S}} \mathbb{T}\cdot \mathrm{d}\boldsymbol{S}, \tag{1}$$

where $\mathbb{T}$ is the stress tensor. Thus, based on the well-known relationship: $\mathbb{P} = -\mathbb{T}$, one can derive the expression for pressure tensor $\mathbb{P}$ by the calculation of $\mathbb{T}$.

Generally, the rate of change of the momentum of the particles in $\boldsymbol{G}$ consists of two contributions. One is the kinetic contribution, which takes into account the change of momentum owing to the entrance and exit of particles through $\boldsymbol{S}$. The other considers the inter-particle potential from the particles beyond the volume $\boldsymbol{G}$. Accordingly, $\mathbb{T}$ can also be decomposed into the kinetic part and configurational part, that is, $\mathbb{T} = \mathbb{T}_K + \mathbb{T}_{\boldsymbol{\Phi}}$. Note that the kinetic part is elementary in the literature, that is, $\mathbb{T}_K = -k_\mathrm{B}T\sum_\nu \rho_\nu(\boldsymbol{r})\mathbb{I}$. Here, k_B, T are respectively the Boltzmann constant and the temperature, and $\mathbb{I}$ is the unit of the tensor. Thus, in what follows, we focus mainly on the derivation of the configurational part $\mathbb{T}_{\boldsymbol{\Phi}}$.

2.1. The configurational contribution $\mathbb{T}_{\boldsymbol{\Phi}}$

For simplicity, only the pair correlation is taken into account in the calculation of the configurational contribution of the stress tensor. Accordingly, the second order phase space probability density function $\wp^{(2)}(\boldsymbol{r}_i, \boldsymbol{r}_j; \boldsymbol{p}_i, \boldsymbol{p}_j)$ is needed in the calculation. In terms of the relation between the force and the potential, the inter-particles force between particles i and j is given by $\boldsymbol{F}_{ij} = -\nabla\varphi(|\boldsymbol{r}_i - \boldsymbol{r}_j|)$. Note that the involved particles may belong to either the same or a different component.

To calculate the configurational contribution of the stress tensor, the force felt by the particles locating in the volume $\boldsymbol{G}$, arising from the particles out of $\boldsymbol{G}$ should firstly be calculated. According to the statistical mechanics, such a force, say $\boldsymbol{F}_{\boldsymbol{\Phi}}$, can be expressed through $\wp^{(2)}(\boldsymbol{r}_i, \boldsymbol{r}_j; \boldsymbol{p}_i, \boldsymbol{p}_j)$ as

$$\begin{aligned}\boldsymbol{F}_{\boldsymbol{\Phi}} = &-\int_{\boldsymbol{G}} \mathrm{d}\boldsymbol{r}_i \int_{\boldsymbol{V}-\boldsymbol{G}} \mathrm{d}\boldsymbol{r}_j \int \mathrm{d}\boldsymbol{p}_i \\ &\times \int \mathrm{d}\boldsymbol{p}_j \boldsymbol{F}_{ij} \wp^{(2)}(\boldsymbol{r}_i, \boldsymbol{r}_j; \boldsymbol{p}_i, \boldsymbol{p}_j).\end{aligned} \tag{2}$$

Due to the fact $\wp^{(2)}(\boldsymbol{r}_i, \boldsymbol{r}_j; \boldsymbol{p}_i, \boldsymbol{p}_j) = \rho^{(2)}(\boldsymbol{r}_i, \boldsymbol{r}_j) f_M^{(2)}(\boldsymbol{p}_i, \boldsymbol{p}_j)$, equation (2) can be rewritten as

$$\begin{aligned}\boldsymbol{F}_{\boldsymbol{\Phi}} = &-\int_{\boldsymbol{G}} \int_{\boldsymbol{V}-\boldsymbol{G}} \nabla\varphi(|\boldsymbol{r}_i - \boldsymbol{r}_j|)\rho^{(2)}(\boldsymbol{r}_i, \boldsymbol{r}_j)\mathrm{d}\boldsymbol{r}_j \mathrm{d}\boldsymbol{r}_i \\ &\times \int\int f_M^{(2)}(\boldsymbol{p}_i, \boldsymbol{p}_j)\mathrm{d}\boldsymbol{p}_j \mathrm{d}\boldsymbol{p}_i.\end{aligned} \tag{3}$$

In fact, it is natural to write momentum distribution function $f_M^{(2)}(\boldsymbol{p}_i, \boldsymbol{p}_j) = f_M^{(1)}(\boldsymbol{p}_i) f_M^{(1)}(\boldsymbol{p}_j)$. Further, by the aid of the normalization condition $\int f_M^{(1)}(\boldsymbol{p})\mathrm{d}\boldsymbol{p} = 1$, equation (3) arrives at

$$\boldsymbol{F}_{\boldsymbol{\Phi}} = -\int_{\boldsymbol{G}} \int_{\boldsymbol{V}} \nabla\varphi(|\boldsymbol{r}_i - \boldsymbol{r}_j|)\rho^{(2)}(\boldsymbol{r}_i, \boldsymbol{r}_j)\mathrm{d}\boldsymbol{r}_j \mathrm{d}\boldsymbol{r}_i, \tag{4}$$

in which the domain $\boldsymbol{V}$–$\boldsymbol{G}$ has been replaced by $\boldsymbol{V}$ in the second integral because the additional integral $\int_{\boldsymbol{G}}\int_{\boldsymbol{G}}$ describes only the total pair force in the volume $\boldsymbol{G}$, which is zero. Note again that in Eq. (4), the coordinate over which the integral is performed can involve the particles of any component. As a consequence, the correlation between different species has been taken into account because the pair potential contains the contribution from either inter- or intra-component.

To proceed, it is convenient to define the relative coordinate $\boldsymbol{r}_{ij} = \boldsymbol{r}_i - \boldsymbol{r}_j$ and the coordinate of mass center $\boldsymbol{r}_c \equiv (\boldsymbol{r}_i + \boldsymbol{r}_j)/2 = \boldsymbol{r}_i - (\frac{1}{2})\boldsymbol{r}_{ij}$. Accordingly, equation (4) can be rewritten as

$$\boldsymbol{F}_{\boldsymbol{\Phi}} = -\int \nabla\varphi(r_{ij})\mathrm{d}\boldsymbol{r}_{ij} \int \rho^{(2)}(\boldsymbol{r}_i - \frac{1}{2}\boldsymbol{r}_{ij}, \boldsymbol{r}_{ij})\mathrm{d}\boldsymbol{r}_i, \tag{5}$$

with $r_{ij} = |\boldsymbol{r}_{ij}|$. Performing Taylor expansion for $\rho^{(2)}(\boldsymbol{r}_i - \frac{1}{2}\boldsymbol{r}_{ij}, \boldsymbol{r}_{ij})$ about $\rho^{(2)}(\boldsymbol{r}_i, \boldsymbol{r}_{ij})$, we have

$$\rho^{(2)}\left(\boldsymbol{r}_i - \frac{1}{2}\boldsymbol{r}_{ij}, \boldsymbol{r}_{ij}\right) = \sum_{\xi=0}^{\infty}\left(-\frac{1}{2}\boldsymbol{r}_{ij}\cdot\nabla_i\right)^{\xi}\rho^{(2)}(\boldsymbol{r}_i, \boldsymbol{r}_{ij}), \quad (6)$$

where ∇_i denotes the derivative with respect to $\boldsymbol{r}_i$. Note that equation (5) is exact because no approximation has been introduced. However, only the first two terms in Eq. (6) are taken into account in this work for simplicity, because the higher order terms contain more complex correlation, which requires the higher order correlation functions to describe.

Accordingly, equation (5) can be approximately rewritten as

$$\begin{aligned}\boldsymbol{F}_{\Phi} &= -\iint \nabla\varphi(r_{ij})\rho^{(2)}(\boldsymbol{r}_i, \boldsymbol{r}_{ij})\mathrm{d}\boldsymbol{r}_{ij}\mathrm{d}\boldsymbol{r}_j \\ &\quad + \frac{1}{2}\int \nabla\varphi(r_{ij})\mathrm{d}\boldsymbol{r}_{ij}\int \boldsymbol{r}_{ij}\cdot\nabla_i\rho^{(2)}(\boldsymbol{r}_i, \boldsymbol{r}_{ij})\mathrm{d}\boldsymbol{r}_i. \quad (7)\end{aligned}$$

The first term equals exactly to zero because it expresses the sum of internal forces between particles in the system at equilibrium. As a consequence, by using of the Gauss theorem, equation (7) can be rewritten as

$$\boldsymbol{F}_{\Phi} = \frac{1}{2}\int \mathrm{d}\boldsymbol{r}_{ij}\nabla\varphi(r_{ij})\int_{\boldsymbol{S}} \boldsymbol{r}_{ij}\cdot\rho^{(2)}(\boldsymbol{r}_i, \boldsymbol{r}_{ij})\mathrm{d}\boldsymbol{S}. \quad (8)$$

Compared with Eq. (1), it is easy to derive the configurational contribution of the stress tensor

$$\mathbb{T}_{\Phi} = \frac{1}{2}\int \frac{\boldsymbol{r}_{ij}\boldsymbol{r}_{ij}}{r_{ij}}\varphi'(r_{ij})\rho^{(2)}(\boldsymbol{r}_i, \boldsymbol{r}_{ij})\mathrm{d}\boldsymbol{r}_{ij}. \quad (9)$$

2.2. The inhomogeneous pressure tensor $\mathbb{P}$

Using the relation $\mathbb{P} = -\mathbb{T}$, we derive the inhomogeneous pressure tensor as follows:

$$\mathbb{P} = k_{\mathrm{B}}T\sum_{\nu}\rho_{\nu}(\boldsymbol{r}_i)\mathbb{I} - \frac{1}{2}\int \frac{\boldsymbol{r}_{ij}\boldsymbol{r}_{ij}}{r_{ij}}\varphi'(r_{ij})\rho^{(2)}(\boldsymbol{r}_i, \boldsymbol{r}_{ij})\mathrm{d}\boldsymbol{r}_{ij}. \quad (10)$$

In general conditions, the system may be exposed to an external potential $V_{\mathrm{ext}}(\boldsymbol{r})$. The presence of $V_{\mathrm{ext}}(\boldsymbol{r})$ also introduces field-induced contribution to $\mathbb{T}$ and then to $\mathbb{P}$. Therefore, the pressure tensor becomes:

$$\begin{aligned}\mathbb{P} &= k_{\mathrm{B}}T\sum_{\nu}\rho_{\nu}(\boldsymbol{r}_i)\mathbb{I} - \frac{1}{2}\int \frac{\boldsymbol{r}_{ij}\boldsymbol{r}_{ij}}{r_{ij}}\varphi'(r_{ij})\rho^{(2)}(\boldsymbol{r}_i, \boldsymbol{r}_{ij})\mathrm{d}\boldsymbol{r}_{ij} \\ &\quad + \sum_{\nu}\rho_{\nu}(\boldsymbol{r}_i)\frac{\boldsymbol{r}_i}{r_i}\nabla_i V_{\mathrm{ext}}(\boldsymbol{r}_i). \quad (11)\end{aligned}$$

This is the main result of this work. Here, the pair density function $\rho^{(2)}(\boldsymbol{r}_i, \boldsymbol{r}_{ij})$ describes the situation when the center of mass of the two-particle pair is at $\boldsymbol{r}_i$, and their relative displacement is $\boldsymbol{r}_{ij}$. It can be generally rewritten as:

$$\rho^{(2)}(\boldsymbol{r}_i, \boldsymbol{r}_{ij}) = \rho\left(\boldsymbol{r}_i + \frac{1}{2}\boldsymbol{r}_{ij}\right)\rho\left(\boldsymbol{r}_i - \frac{1}{2}\boldsymbol{r}_{ij}\right)g(r_{ij}), \quad (12)$$

where the radial distribution function (RDF) $g(r_{ij})$ takes into account the correlation between particles. Further, $\rho(\boldsymbol{r}_i \pm \frac{1}{2}\boldsymbol{r}_{ij})$ in Eq. (12) can be expanded about the density r_i as follows:

$$\rho\left(\boldsymbol{r}_i \pm \frac{1}{2}\boldsymbol{r}_{ij}\right) = \rho(\boldsymbol{r}_i) \pm \frac{1}{2}(\boldsymbol{r}_{ij}\cdot\nabla_i)\rho(\boldsymbol{r}_i) + \text{h.o.t.} \quad (13)$$

Combining Eqs. (11)–(13), the inhomogeneous pressure tensor can be numerically calculated once the density $\rho_{\nu}(\boldsymbol{r})$ is obtained. Note that equation (11) is different from the IK definition[4] because the second term contains the correlation between different components. Moreover, it is also different from the derivation by Bearman and Kirkwood,[22] who had underestimated the correlation between particles, because they used a mean field treatment, that is $\rho^{(2)}(\boldsymbol{r}_i, \boldsymbol{r}_{ij}) = \rho(\boldsymbol{r}_i)\rho(\boldsymbol{r}_i)g(r_{ij})$, in their final expression.

3. Results and discussion

Note that in this work, we focus on the pressure tensor of the fluid mixture. The theoretical derivation is applicable to the systems with various inter-particle potential. Actually, both experimental and theoretical studies have shown that the short-ranged correlation plays a decisive role in determining the structure or thermodynamic properties of the real fluids. Therefore, the HS fluid has been widely used as a reference system in the studies of these real systems. Especially in the colloidal suspension, the colloidal particle can be directly modeled by a hard sphere with an effective diameter.[44–47] To this end, the pressure tensor in the binary HS mixture is focused on in this paper, and the influences of volume fraction and size asymmetry are investigated in detail.

As shown in Eq. (11), the RDFs is necessary in the calculation of the pressure tensor in the mixture. However, due to the hard sphere potential in our chosen system, the derivative $\varphi'(r_{ij}) = -k_{\mathrm{B}}T\delta(r_{ij} - \sigma_{ij})$ with $\sigma_{ij} = (\sigma_i + \sigma_j)/2$, which suggests that only the contact value of the RDFs is needed. Therefore, in the calculations, we have employed the expression of the RDFs for the hard sphere mixture, which is derived by Lebowitz.[48] In addition, for simplicity in calculations, we have replaced the RDFs with those of the uniform system with the densities the same as those in their bulk phases.

Firstly, to evaluate our theoretical derivation and the numerical calculations, we applied our main result to the one-component HS fluids, and compare our results with those from the molecular dynamics (MD) simulation performed by Lupkowski *et al.*[44] In the calculation for the tangential pressure, the HS fluid is surrounding a large sphere of the radius $R_{\mathrm{b}} = 30\sigma$ with σ the diameter of the small HS. Note that R_{b} is large enough in order to approach the limit of a flat wall. The bulk density is set as $\rho_{\mathrm{b}}\sigma^3 = 0.763641$ to produce the normal pressure $P_{\mathrm{N}}\sigma^3/\varepsilon = 5.284$. Here ρ_{b} is the bulk density of the HS fluid. The comparison shown in the Fig. 1(a) suggests that

the agreement between our result and the MD result is rather good.

In the further calculations, we take $t = 2$, which corresponds to a binary mixture. For simplicity, both inter- and intra-component interactions are modeled by the HS potential. By definition, the binary HS mixture is composed of the small and big components, which have the diameter σ_s and σ_b, respectively. The total volume fraction is defined as $\eta_{tot} \equiv \eta_s + \eta_b$ with $\eta_\nu = \frac{1}{6}\pi\rho_{b,\nu}\sigma_\nu^3$ and $\rho_{b,\nu}$ the bulk density of the ν-th component. To calculate the pressure profile for the binary HS mixtures, the density of each component should be firstly calculated. To check our calculation for the density profiles in binary mixture with MFMT,[38,39] the results are compared in Fig. 1(b) with those from the Monte Carlo simulation performed by Kim *et al.*[50] In the calculation, we set $\sigma_b/\sigma_s = 2.0$, $N_s = 67$, and $N_b = 16$. The comparison shown in Fig. 1(b) suggests that the two sets of results agree well with each other.

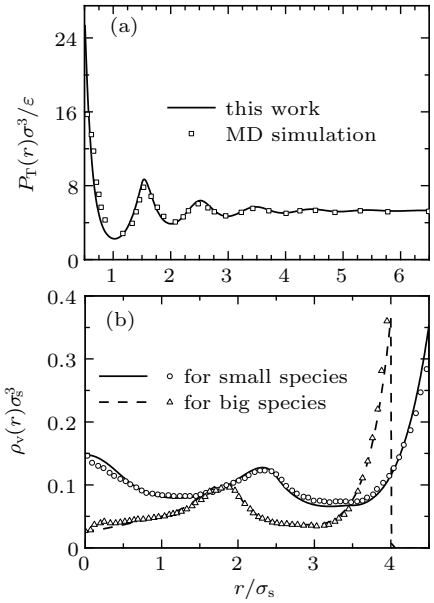


Fig. 1. (a) Comparison of our numerical results of the tangential components of the pressure tensor with those from the MD simulation.[49] (b) Comparison of the calculated density profiles in the mixture with those from the MC simulation.[50]

3.1. Effect of the total volume fraction

For the hard sphere mixtures under consideration, the excluded volume determines the structure and pressure tensor in it. So, the properties of the system should be very sensitive to the total volume fraction, say η_{tot}. Then, to understand how η_{tot} influences the profile of the pressure components, we calculate the normal and tangential components of the inhomogeneous pressure tensor in a spherical cavity with a radius of $R_c = 10\sigma_s$. In the calculation, we set the ratio $z \equiv \eta_s/\eta_{tot} = 0.5$, size ratio $\sigma_b/\sigma_s = 2.0$. The results under the conditions of $\eta_{tot} = 0.1$, 0.2, 0.3, 0.4 are given in Fig. 2. Moreover, to show the relationship between the pressure profile and the structure, we also plot the corresponding density profiles in the figures.

Our results suggest that when η_{tot} is small, such as $\eta_{tot} = 0.1$ in Fig. 2(a), both the normal and tangential pressure show a uniform profile in the central region of the cavity. This should be attributed to the uniform profile of the density profile of the mixture in this region. However, as the magnitude of η_{tot} is increased, the curves for pressure profiles show oscillation in the central region. Through the comparison between results shown in Figs. 2(b)–2(d), it is obvious that the bigger the magnitude of η_{tot} is, the more significant the oscillation is.

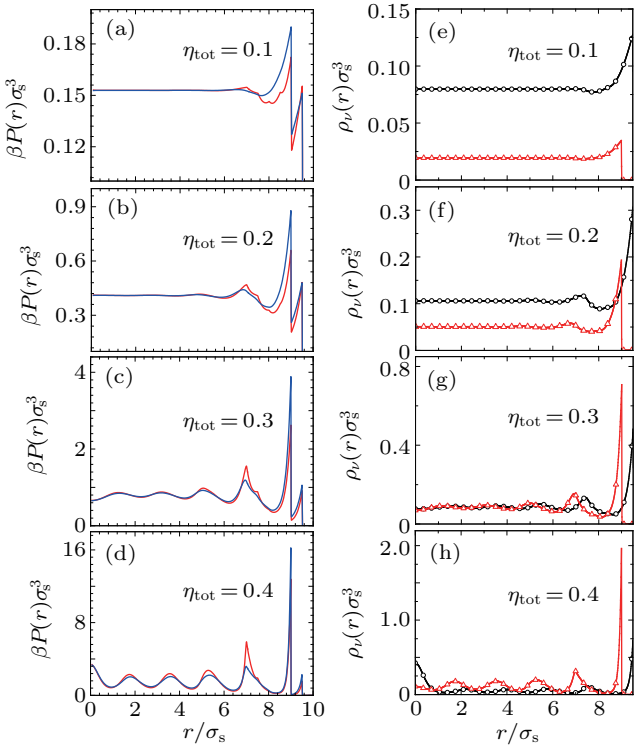


Fig. 2. (color online) Profiles of normal and tangential components of the pressure tensor under different conditions of η_{tot}. In panels (a)–(d), the red and blue lines give respectively the results for normal and tangential pressure. Panels (e)–(h) plot the density profiles of the corresponding mixture.

Moreover, as shown in Fig. 2, a discontinuous profile for both pressure components is observed, which locates at the point $\sigma_b/2$ from the wall. In fact, the region $(R_c - \sigma_b/2, R_c)$ is inaccessible for the big sphere because of the existence of the cavity wall at the position R_c. Therefore, in this region, the interaction between big–big pairs is absent, and only the big–small and small–small pairs can contribute to the pressure. This is responsible for the discontinuity in the pressure profiles. In addition, in the region not very far from the cavity wall, the curves for both pressure components are not as smooth as those in the central region. This may arise from the separation of the outermost layers for both components in the mixture.

3.2. Effect of the ratio of volume fraction

In the hard sphere mixture, due to the correlation between particles, the variation of the fraction of each component may

lead to significant changes in both structural and thermodynamic properties. In order to understand the influence of ratio of volume fraction on the pressure components, we have performed the calculation under different conditions of z, with the given $\eta_{\rm tot} = 0.3$ and $\sigma_{\rm b}/\sigma_{\rm s} = 2.0$. The results for $P_{\rm N}(r)$ and $P_{\rm T}(r)$ are respectively given in Figs. 3(a) and 3(b).

Our results suggest that for the given $\eta_{\rm tot}$ and $\sigma_{\rm b}/\sigma_{\rm s}$, both pressure components are very sensitive to the magnitude of z. Specifically, when z is small, both pressure components are relatively small, while as z is increased, the value of both $P_{\rm N}(r)$ and $P_{\rm T}(r)$ are enhanced in the whole region. This can be understood by the microscopic mechanism of the pressure tensor in statistical mechanics, which interprets the pressure tensor as a statistical average of the inter-particle force across a given area. For the smaller value of z, most of the space in the cavity is occupied by the big sphere, which indicates a smaller number of the particle pair in the system, and then leads to the reduction of the inter-particle force across a given position. On the contrary, as the value of z is increased, the total particle number $N = N_{\rm s} + N_{\rm b}$ is also increased, which results in the increase of particle pair, and then the values of pressure components. Moreover, when z is small, it is also obvious that both components can be nearly uniform in the central region. This can also be explained by the smaller value of the total particle number N, which gives almost a bulk phase in the central region.

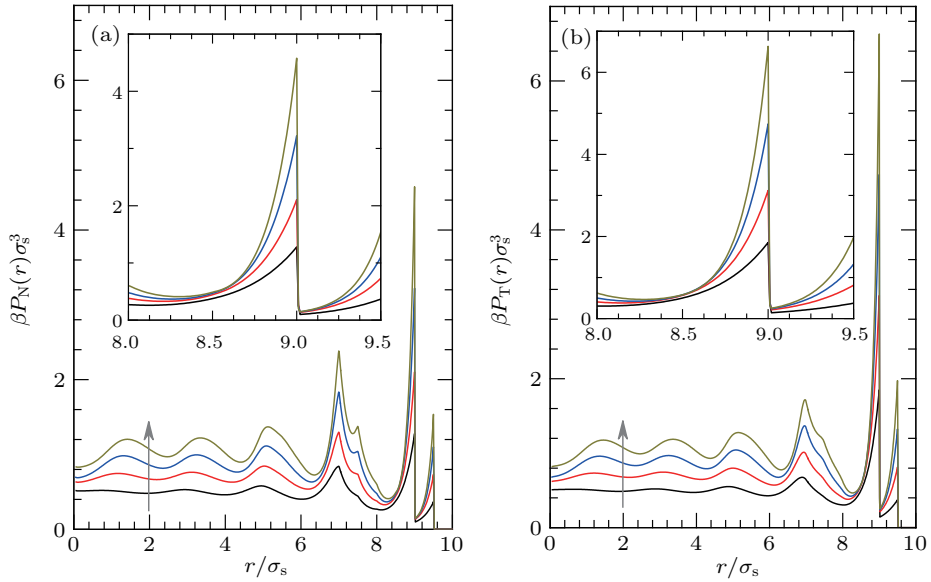


Fig. 3. (color online) Profiles of normal and tangential components of the pressure tensor under different conditions of ratio of volume fraction. Along the arrow in both figures, the curves correspond respectively to $z = 0.2, 0.4, 0.6, 0.8$.

Comparison between the results for $P_{\rm N}(r)$ and $P_{\rm T}(r)$ suggests that in the central region of the cavity, both pressure components are almost the same due to the decay of the influence of the cavity wall. In addition, the results in the inset show that with the increase of z, the jump locates at $R_{\rm c} - \sigma_{\rm b}/2$ in the curves is raised.

3.3. Effect of the size asymmetry

In the fluid mixture, the size ratio, say $\sigma_{\rm b}/\sigma_{\rm s}$, may play an important role in determining the structure of the system. Especially, the depletion induced attraction between big spheres relates not only to the volume fraction of small spheres, but also to the size ratio of particles in the two components. Due to the close relationship between the structure and pressure tensor, it is believed that the size ratio may show significant influence on the pressure profile in the confined mixture. Therefore, in this section, we calculate the profiles of $P_{\rm N}(r)$ under different conditions of the size ratio, with the given $\eta_{\rm tot} = 0.3$ and $z = 0.5$. The results for $P_{\rm N}(r)$ are given respectively in Fig. 4.

In our calculation, both $\eta_{\rm tot}$ and z are simultaneously given, which indicates that the number of small spheres is fixed. In such a situation, the smaller size ratio corresponds to a larger number of big spheres in the cavity. Therefore, more particle pairs provide the force that passes across the given point, and then contribute more to the pressure there. In addition, it should be mentioned that when $\sigma_{\rm b}/\sigma_{\rm s} = 1.0$, the discontinuity disappears in the curves because of the fact that in this case, the system is actually composed of only one single component.

Further, from the results shown in the inset, it is obvious that the pressure at the position $R_{\rm c} - \sigma_{\rm b}/2$ is enhanced when the size ratio is increased. This may arise from the enhanced depletion, which pulses the big sphere to the region near the cavity wall. Moreover, it is interesting that the pressure is nearly uniform in the central region when the size ratio is small, while it is in an oscillating pattern when the size ratio is large. As mentioned above, when the size ratio is large,

the big sphere gathers in the region near the cavity wall. In the meanwhile, most of the small spheres are excluded to the central region to form an oscillating structure.

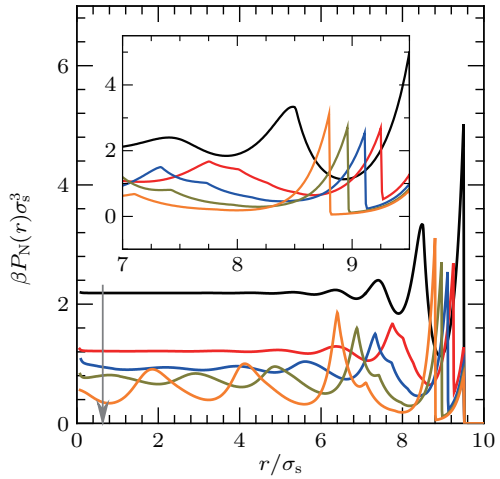


Fig. 4. (color online) Profiles of normal component of the pressure tensor under different conditions of size asymmetry. Along the arrow in the figure, the curves correspond respectively to $\sigma_b/\sigma_s = 1.0$, 1.5, 1.8, 2.1, 2.4.

3.4. Mixture confined in a soft cavity

In all the above calculations, the hard sphere mixtures are confined in the hard cavity. The significant influence of the wall on both the structure and the pressure has been displayed by their maximum in the region near the wall. In fact, this is the result of the depletion between the particles and the wall. In the following, we turn to the binary mixture confined in a cavity with a soft wall, which provides an external potential $V_{ext}(r)$ for both species:

$$V_{ext}(r) = \varepsilon \left(\frac{r}{w}\right)^{15}, \tag{14}$$

with $w = 0.6R_c$ and ε the unit of the potential. The exponent number is so large that it is safe to regard the wall as a hard one when the particle is close enough to it.

Firstly, we perform calculations to investigate the influence of z on the pressure and density profiles. In the calculation, we set $\varepsilon = 1.0$, $\eta_{tot} = 0.3$ and $\sigma_b/\sigma_s = 2.0$. The results are given in Figs. 5(a)–5(d). Our results suggest that the pressure profile is enhanced with the increase of z, which is similar to the situation of a hard cavity. However, as the magnitude of z is increased, the peaks in the both pressure profiles are slightly shifted outwards. A similar phenomenon can also be observed in the curves for a density profile of big species, which is given in Fig. 5(d). Actually, the depletion induced gathering of the big species in the outer region is responsible for the shift of the peaks.

Obviously, in the soft cavity, the discontinuity in the pressure profiles disappears, which is in sharp contrast with the condition of the hard cavity. This can be understood with the aid of the corresponding density profiles, which are shown in Figs. 5(c) and 5(d). In fact, the soft cavity provides each species with a soft and continuous external potential, which is different from the contact potential provided by the hard wall. In such a situation, the density profiles of both species should also be smooth in its accessible space, which in turn leads to the smooth profile of the pressure.

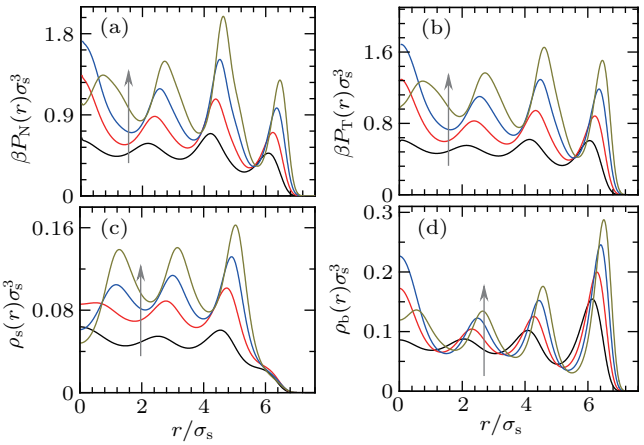


Fig. 5. (color online) (a) and (b): Profiles of normal and tangential components of the pressure tensor under different conditions of ratio of volume fraction. (c) and (d): Density profiles for the small and big components confined in the soft cavity. Along the arrow in the figure, the curves correspond respectively to $z = 0.2$, 0.4, 0.6, 0.8.

Moreover, we have also calculated the influence of size ratio on the pressure profiles in the soft cavity with $\varepsilon = 1.0$, $\eta_{tot} = 0.3$ and $z = 0.5$. Comparing the results in Fig. 6, it is easy to find that when the size ratio is small, the pressure in the central region is nearly uniform. However, as the size ratio is increased, the pressure profile turns into an oscillation pattern, especially in the region near the center of the cavity. This is similar as that in the situation of the hard cavity.

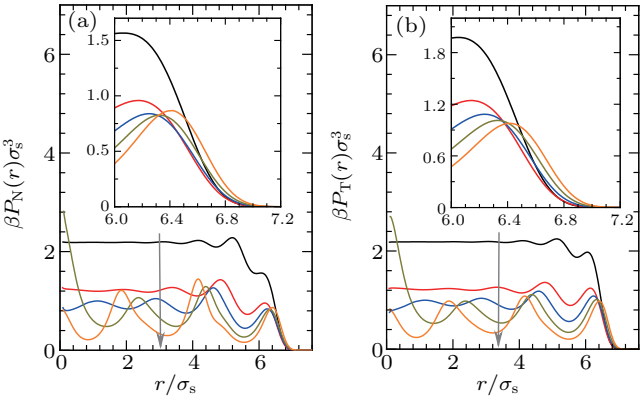


Fig. 6. (color online) Profiles of normal and tangential components of the pressure tensor under different conditions of size asymmetry. Along the arrow in the figure, the curves correspond respectively to $\sigma_b/\sigma_s = 1.0$, 1.5, 1.8, 2.1, 2.4.

4. Conclusion

In summary, the pressure tensor of an inhomogeneous fluid mixture is derived. In the theoretical derivation, the pressure tensor has been expressed as a functional of the density function, which can be obtained by using density functional

theory. In this work, the binary hard sphere mixture confined in the hard cavity is firstly studied, and the numerical results for both normal and tangential components of the pressure tensor are given. The influences of total volume fraction, ratio of volume fraction, and size asymmetry on the pressure are analyzed in detail.

The results show that for the mixture with a size imbalance, a discontinuity on the profile of the pressure can usually be observed. Our results suggest also that the oscillation of both pressure components is enhanced when the total volume fraction is increased. Besides, a larger ratio of volume fraction is also beneficial for the oscillation of the pressure profiles. In addition, the size ratio is helpful for the inhomogeneity of the pressure, while it leads usually to a smaller value of the pressure. Additionally, the hard sphere mixture confined in a soft cavity is also studied. The results suggest that the discontinuity in the pressure profile disappears, which is in sharp contrast with the case of the hard cavity.

To be fair, in this work, some approximation has been introduced before performing the calculations; however, the comparison between our results and those from the computer simulation suggests that our treatment could provide a reliable result. Therefore, it is hoped that our results can provide useful clues in understanding the hydrodynamics and thermodynamics of fluids at the nanoscale.

References

[1] Rowlinson J S and Widom B 1982 *Molecular Theory of Capillarity* (Oxford: Clarendon Press)
[2] Croxton C A 1986 *Fluid Interfacial Phenomena* (New York: Wiley)
[3] Davis H T and Scriven L E 1982 *Adv. Chem. Phys.* **49** 357
[4] Irving J H and Kirkwood J G 1950 *J. Chem. Phys.* **18** 817
[5] Hafskjold B and Ikeshoji T 2002 *Phys. Rev. E* **66** 011203
[6] Iwamatsu M 2003 *Physica A* **329** 14
[7] Brodskaya E N and Rusanov A I 2009 *Colloid Journal* **71** 22
[8] Long Y, Palmer J C, Coasne B, Sliwinska-Bartkowiak M, Jackson G, Müller E A and Gubbins K E 2013 *J. Chem. Phys.* **139** 144701
[9] Schofield P and Henderson J R 1982 *Proc. R. Soc. Lond. A* **379** 231
[10] Harasima A 1958 *Adv. Chem. Phys.* **1** 203
[11] Thompson A P, Plimpton S J and Mattson W 2009 *J. Chem. Phys.* **131** 154107
[12] Wang Z, Liu L C and Neretnieks I 2011 *J. Chem. Phys.* **135** 244107
[13] Nakamura T, Shinoda W and Ikeshoji T 2011 *J. Chem. Phys.* **135** 094106
[14] Heyes D M, Smith E R, Dini D and Zaki T A 2011 *J. Chem. Phys.* **135** 024512
[15] Eslami H and Mehdipour N 2012 *J. Chem. Phys.* **137** 144702
[16] Coasne B, Long Y and Gubbins K E 2014 *Mol. Simul.* **40** 721
[17] Milchev A 2015 *J. Chem. Phys.* **143** 064701
[18] Wang Z, Liu L C and Neretnieks I 2015 *Mol. Phys.* **114** 599
[19] Todd B D, Evans D J and Daivis P J 1995 *Phys. Rev. E* **52** 1627
[20] Cormier J, Rickman J M and Delph T J 2001 *J. Appl. Phys.* **89** 99
[21] Sun Z L, Kang Y S, Kang Y M, Liu Z C and Ma H X 2012 *Chin. Phys. B* **21** 066103
[22] Bearman R J and Kirkwood J G 1958 *J. Chem. Phys.* **28** 136
[23] Harris R A and Rice S A 1960 *J. Chem. Phys.* **33** 1047
[24] Snell F M, Aranow R and Spangle R A 1967 *J. Chem. Phys.* **47** 4959
[25] Evans R 1979 *Adv. Phys.* **28** 143
[26] Henderson D 1992 *Fundamentals of Inhomogeneous Fluids* (New York: Dekker)
[27] Hansen J P and McDonald I R 1986 *Theory of Simple Liquids* (New York: Academic)
[28] Ramakrishnan T V and Yussouf M 1979 *Phys. Rev. B* **19** 2775
[29] Calleja M, North A N, Powels J G and Rickayzen G 1991 *Mol. Phys.* **73** 973
[30] Zhou S Q and Ruckenstein E 2000 *Phys. Rev. E* **61** 2704
[31] Zhou S Q and Ruckenstein E 2000 *J. Chem. Phys.* **112** 8079
[32] Choudhury N and Ghosh S K 2001 *J. Chem. Phys.* **114** 8530
[33] Kim S C and Suh S Y 2002 *J. Chem. Phys.* **117** 9880
[34] Zhou S Q 2008 *Chin. Phys. B* **17** 3812
[35] Tarazona P 1985 *Phys. Rev. A* **31** 2672
[36] CurtinW A and Ashcroft N W 1985 *Phys. Rev. A* **32** 2909
[37] Rosenfeld Y 1989 *Phys. Rev. Lett.* **63** 980
[38] Yu Y X and Wu J Z 2002 *J. Chem. Phys.* **117** 10156
[39] Roth R, Evans R, Lang A and Kahl G 2002 *J. Phys.: Condens. Matter* **14** 12063
[40] Yu Y X, You F Q, Tang Y P, Gao G H and Li Y G 2006 *J. Phys. Chem. B* **110** 334
[41] Yu Y X 2009 *J. Chem. Phys.* **131** 024704
[42] Cao D P, Cheng L S and Wang W C 2007 *Chin. Phys.* **16** 2296
[43] Xu X F and Cao D P 2010 *J. Chem. Phys.* **133** 121101
[44] Pusey P N and van Megen W 1986 *Nature* **320** 340
[45] van Blaaderen A and Wiltzius P 1995 *Science* **270** 1177
[46] Royall C P, Louis A A and Tanaka H 2007 *J. Chem. Phys.* **127** 044507
[47] Royall C P, Poon W C K and Weeks E R 2013 *Soft Matter* **9** 17
[48] Lebowitz J L 1964 *Phys. Rev.* **133** A895
[49] Lupkowski M and van Swol F 1990 *J. Chem. Phys.* **93** 737
[50] Kim S C, Suh S H and Lee C H 1999 *J. Korean Phys. Soc.* **35** 350